Modeling of landslides in Valles Marineris, Mars, and implications for initiation mechanism

Meaza Tsige [a,*], Javier Ruiz [a], Ian A. del Río [a,b], Alberto Jiménez-Díaz [a]

[a] *Departamento de Geodinámica, Facultad de Ciencias Geológicas, Universidad Complutense de Madrid, 28040 Madrid, Spain*

[b] *Departamento de Ciencias Geológicas, Universidad Católica del Norte, Antofagasta, Chile*

* Corresponding author:

Meaza Tsige

+34 91 394 4815

+34 91 394 4845

meaza@geo.ucm.es

The Valles Marineris canyon system in Mars shows large landslides across its walls, which can be 40 km wide and up to 60 km long, with fall scarps height as high as 7 km. These landslides were produced through a large mass movement at high speed by gravity across the trough floor. Although the triggering factors are unclear, several mechanisms have been proposed as, among others, large amounts of subsurface water, quake produced through normal faulting close to the canyon walls, and meteoritic impacts. In this work we examine the limit equilibrium slope stability of three landslides (placed respectively at Ius, Candor, and Melas Chasmata), which can be considered representative, with the aims of constraining their formation conditions. Our results

suggest that external factors (as high pore fluid pressure, seismic loading or rock mass disturbance) do not seem necessary for the failure of slopes if they are composed of unconsolidated materials, while high pore water pressure or ground acceleration are needed to trigger slides in slopes composed of strong basaltic-like materials. Moreover, the presence of sub-surface ice would contribute to slope stability. As a whole, our findings point to ground shaking due to meteorite impacts as the main triggering force for most landslides in the Valles Marineris.

Mars; Martian landslides; Valles Marineris; groundwater

1 Introduction

Mars is roughly half the size of Earth but many of its geomorphologic and tectonic landforms are substantially larger than those of Earth. Valles Marineris forms an immense east-west-trending, 4500-km-long canyon system of tectonic origin (with magmatic influence), and affected by water action (e.g., Lucchita et al. 1992; Schultz 1998; Dohm et al. 2009). On its floor, the trough displays large landslides generated from the wall rock with lengths and widths reaching 60 km and 40 km, respectively, as well as scarps up to 7 km (Quantin et al. 2004a). The long-runout subaerial mass movement is one of the most prominent geomorphic processes shaping Valles Marineris. The role of basal lubrication by water, ice, snow, evaporites or dry granular flow in this long-distance transport has been debated for decades. In a recent study Watkins et al. (2015), indicate morphological and structural evidence of pervasive deformation at Ius Chasma, suggesting the presence of minerals such as possibly phyllosilicates in the outer zones of the landslides that could have played a decisive role in facilitating landslide transport by lubricating the basal sliding zone.

The forces that triggered the landslides have also generated large discussion. The discovery of ice in the Martian subsurface (Boynton et al. 2002;

Möhlmann 2004) has prompted many authors to propose ice melt as the main landslide trigger (Mangold et al. 2000; Harrison and Grimm 2003; Wang et al. 2005; De Blasio 2012). In contrast, other authors suggest slope failure under dry static conditions (yielding transverse ridge morphologies and hummocky structures) as sufficient to mobilize materials without the need for elevated surface or subsurface water. Consistent with this hypothesis, several works attribute a key role in initiating slides to tectonic control through normal faulting close to landslide scarps (Peulvast et al. 2001; Schultz 2002; Quantin et al. 2004a), or to meteoritic impacts generating seismic waves and ground acceleration (Soukhovitskaya and Manga 2006). Neuffer and Schultz (2006) suggested the need for elevated pore-fluid pressures or ground acceleration, or both, to trigger landslides at the slopes composed of competent rock materials such as possibly basalt. These two mechanisms could arise from meteoritic impacts, and when coupled with seismic forces, would imply a heat mechanism to liquefy the ice possibly present in the first few kilometers of the Martian surface leading to increased pore-fluid pressure. Brunetti et al. (2014) also concluded that an external energy source is necessary to produce the landslides observed in Valles Marineris.

Recently, Lucas et al. (2011) assessed the effects of the initial geometry of the fractured surface on the dynamics of landslides and the volume of mobilized material. Crosta et al. (2014) addressed the stability of the slopes of the canyon walls of Valles Marineris, constraining the mechanical properties of the rock masses forming the rock walls and affected by landslides, suggesting that rock masses have comparable strengths to their Earth equivalents. These authors concluded that rocky materials comprising slopes must be highly affected by seismic loading produced by meteoritic impacts. The damage of these materials would lead to weaker mechanical properties even at great depths.

In this work, we investigated the triggering mechanism of the landslides through limit equilibrium slope analysis of three representative landslides (Fig. 1 and Fig. 2). In addition, our study sought to determine the conditions and mechanisms that are necessary to initiate the three representative landslides using a parametric slope stability analyses and reportedly appropriate lithological

materials. Our analysis, which investigates the effects of material strength, groundwater amount, rock mass disturbance and external forces, is based on the methodology described by Abramson et al. (2001) and Neuffer and Schultz (2006). Finally, we discuss the implications of our results regarding existing models of landslide formation and subsurface conditions on Mars.

2 Studied landslides

As mentioned above, there are several large landslides associated with prominent scarps of Valles Marineris (Quantin et al. 2004a; Brunetti et al. 2014). These landslides likely involve materials of ranging characteristics and lithologies, probably from high strength basalts to low resistance piroclasts (Lucchitta 1999; McEwen et al. 1999; Chapman 2002; Hynek et al. 2003; Komatsu et al. 2004; Bigot-Cormier and Montgomery 2007). In this work we examine three landslides (placed respectively at Ius, Candor, and Melas Chasmata; Fig. 2), which can be considered representative because their complementary geomorphologic characteristics. The selection of the landslides for geomorphologic characterization was performed using both Context Camera (CTX) and the High Resolution Imaging Science Experiment (HiRISE) images acquired from the Mars Reconnaissance Orbiter (MRO) spacecraft.

The first landslide that we examined is located in Ius Chasma, a canyon of the western part of Valles Marineris (Fig. 2a). This landslide, which is estimated to be >1 Ga based on crater statistics (Quantin et al. 2004b), extends nearly 50 km onto the opposing slope and has a width surpassing 100 km. Scarp tops exceed 5000 m above reference level, while the canyon floor occurs at some -500 m and -2000 m, respectively in the western and eastern parts of the landslide. This landslide consists entirely of large blocks; those larger in size reach lengths of 6 km and are covered by eolian dunes. The scarp slope is estimated to range from 40% to 45%, while adjacent non-failed slopes from 43% to 35%. Minor landslides with distinct flow features appear in zones closest to the scarp. In the upper 2000 m of the scarp, layered stratigraphy is exposed in the walls of Ius Chasma; such stratification here and elsewhere has been interpreted to be igneous rocks with

intercalations of competent basalt and poorly resistant materials (including pyroclasts or hyaloclastite) (McEwen et al. 1999; Komatsu et al. 2004; Dromart et al. 2007). The rest of the scarp appears to be covered by remobilized materials.

The second examined landslide, estimated to have formed 0.2 Ga (Quantin et al. 2004b), is located in the northwest part of Candor Chasma (Fig. 2b). This landslide is distally confined by a stratified plateau. Its run-out distance is 25 km and the width of its central region is 20 km, though owing to the presence of the plateau, its width decreases distally to give the landslide a triangular shape. This landslide also has a vertical drop of about 4800 m. While the top and scarp of the landslide display many features common to the investigated landslide of Ius Chasma, it differs in terms of the composing slide materials. For example, though this landslide likewise comprises many broken blocks, its main body consists of smaller blocks giving it a gentler topography.

The third examined landslide, estimated as 1 Ga old (Quantin et al. 2004b), is located in Melas Chasma (Fig. 2c). This landslide is laterally confined by mountainous crests that span from the base of the canyon system to the top of the plateau (Ophir Planum) which partly encompasses its source area. This configuration confines the main body of the slide, composed of blocks hundreds of meters in length, from reaching the main part of the canyon floor (leaving it "hanging"). Otherwise, the landslide's scarp is smaller than the two other examined landslides, with a height difference of around 3000 m between the slide top and the failed material at the bottom. At the top of the scarp, rock materials can be seen projecting out of the canyon wall. The slide distal region (run-out), which extends as far as 74 km, displays distinctive flow morphologies.

The three analyzed landslides are hereafter referred to as Ius Chasma, Candor Chasma and Melas Chasma landslides. The failure surfaces of these landslides are circular, especially observed in the present-day morphology of the Ius and Melas Chasmata (see Section 3). A feature common to the three landslides is the presence of multiple fractured surfaces of constant diameter. This suggests a landslide integrated by several smaller slides occurring at the same time or within a short time period (Quantin et al. 2004b), which is supported by the presence of

clearly overlapping lobes that have nevertheless a similar age (Quantin et al. 2004b).

3 Slope stability analysis

For slope stability analysis of the three studied landslides, we used a simplified limit equilibrium analysis, which estimates the vertical force equilibrium for the slice of slipped material and the overall moment equilibrium about the center of the circular failure surface (Abramson et al. 2001). We investigate the safety factor (*SF*) of the appropriate slope as a function of the initial slope characteristics and properties of the material assumed to be representative of Martian conditions. For $SF < 1$, the slope is unstable, and a landslide can occur.

We perform a parametric slope stability analyses adjusting realistic geometry of the failure surface to the initial pre-failure geometry of the landslide walls. Thus, we first define a geometrical model of the initial slope for each of three analyzed landslides, based on Mars Orbiter Laser Altimeter (MOLA) topography (Smith et al. 2001) of the adjacent, non-slipped, canyon walls (Fig. 3). To estimate the safety facto , we did the following: (1) introduced a failure surface with rotational movement deduced from the geomorphologic evidence observed in the walls of Valles Marineris, and (2) allowed the program to generate the lowest safety factor.

The safety factor was estimated for the initial slope of each of the three studied landslides from varying the values of three key parameters: water pressure (*Ru*), disturbance factor (*D*), and seismic load coefficient (*SLC*). The water pressure is defined as the ratio between the pore fluid pressure at a point in the rock mass and the lithostatic pressure at that same point. In this work we consider *Ru* values between 0 and 1; *Ru* values of 0 and 0.5 indicate, respectively, dry and saturated conditions in the slope, whereas values higher than 0.5 were used to examine the effect of possible existence of excess pore water pressure as landslide triggering factor or stress reduction element. The disturbance factor, *D*, is a

measure of the potential modifications in the rock mass related to triggering factors (Hoek et al. 2002), and accounts for the weakened rock mass due to numerous meteoritic impacts near a particular wall of Valles Marineris (Crosta et al. 2014; Frattini et al. 2014). Thus, we consider *D* values between 0 and 1 for, respectively, undisturbed in situ rock masses properties and highly disturbed mechanical properties in the landslide failure models. On the other hand, the seismic load coefficient (*SLC*) is a measurement of horizontal ground acceleration in the movement direction. Previous works suggested that the activity of normal faults close to landslide scarps and/or the numerous meteoritic impacts could produce an important ground motion near the slopes, which can exceed the estimated critical acceleration value of about $0.2g_M$ (Bigot-Cormier and Montgomery, 2007) (where g_M = 3.72 m s^{-2} is the Martian gravity), and hence contribute to trigger some of the Valles Marineris landslides. To evaluate these conditions, the three slopes were modeled assuming *SLC* values between 0 and 1.5 g_M; extreme *SLC* values similar to the ones Earth. It is worth mentioning that the acceleration force contributes mainly as vertical and horizontal driving forces at the slope surface.

Considered appropriate for Mars (Neuffer and Schultz, 2006), six different classes of materials were used in the analysis, ranging from strong-very strong rocks similar to basalt and gabbro, to weak-very weak rocks as non-welded tuffs or fractured hyaloclastite, with their geotechnical properties shown in Table 1. Also, we assume isotropic and homogeneous behavior of the materials across the entire slope.

In order to determinate SF for the cases involving the properties of sandstone, non-welded tuff, welded tuff, hyaloclastite, basalt, and gabbro, we use the Hoek and Brown failure criterion for isotropic materials (Hoek et al. 2002; Eberhardt 2012), defined by:

$$\sigma_1 = \sigma_3 + \sigma_c\left(mi\frac{\sigma_3}{\sigma_c} + s\right)^{\alpha}, \qquad (1)$$

where σ_1 and σ_3 are the main maximum and minimum stress, σ_c is the simple compression strength of the rock, and *mi*, *s* and α are non-dimensional constants that depend on the rock mass.

On the other hand, for the fractured hyaloclastite (representative of soil-like materials), we apply the Mohr-Coulomb failure criterion:

$$\tau = c + \sigma_n \tan(\varphi), \qquad (2)$$

where τ is the shear stress, σ_n is the normal stress, *c* is cohesion, and φ is the angle of internal friction (*c* and φ for fractured hyaloclastite are shown in Table 1).

4 Results

The modelled slope stability varies widely according to the lithology used in the calculations (see Table 2 for $D = 0$, and Table 3 for $D = 1$). For slopes composed of intact basalt or gabbro (both highly resistant) and $D = 0$, $Ru = 0$ and $SLC = 0\ g_M$, we obtain *SF* values greater than 3.8 (even greater than 7 in the case of the Candor Chasma landslide), precluding the possibility of slope failure; slope instability ($SF < 1$) was only observed for $Ru > 0.8$-0.9 or $SLC > 0.6$-$1.3\ g_M$, with the exact lower limits depending on each landslide (because of the differences in the geometries of the examined slopes). For $D = 1$, $Ru = 0$ and $SLC = 0\ g_M$, the obtained *SF* ranges from 2 to 5, yet somewhat greater for slopes assumed to be formed by a gabbro lithology; slope instability ($SF < 1$) was only observed for $Ru > 0.6$-0.8 or $SLC > 0.3$-$0.8\ g_M$. Thus, instability for basalt-like materials requires high amounts of subsurface water (higher than saturation) or significant ground accelerations.

When slopes of hyaloclastite breccia-like materials (i.e., weak rocks) are considered, our results are more variable and, taking $Ru = 0$ and $SLC = 0\ g_M$, yield

SF values from 2.7 to 5.2 for $D = 0$, and from 1.6 to 3.2 for $D = 1$. These results indicate that: for undisturbed conditions, slope instability would need $Ru > 0.7\text{-}0.9$ or $SLC > 0.6\text{-}0.8\ g_M$, whereas conditions with $D = 1$, slope instability would require $Ru > 0.5\text{-}0.8$ or $SLC > 0.2\text{-}0.5\ g_M$. These results are similar, maybe slightly weaker, than those obtained for basalt-like materials. Slopes modeled using hyaloclastite fracture-like lithologies are much more unstable, with *SF* values between 0.8 and 1.7 for both undisturbed and disturbed conditions. In general, slope instability does not require highly restrictive conditions: $Ru > 0.0\text{-}0.4$ or $SLC > 0.0\text{-}0.3\ g_M$ for $D = 0$, and $Ru > 0.0\text{-}0.4$ or $SLC > 0.0\text{-}0.1\ g_M$ for $D = 1$.

For slopes modeled using the properties of welded tuffs, taking $Ru = 0$ and $SLC = 0\ g_M$, we obtain *SF* values from 0.8 to 1.5 for $D = 0$, and from 0.1 to 0.3 for $D = 1$. Thus, for $D = 0$ slope instability would require $Ru > 0.0\text{-}0.5$ or $SLC > 0.0\text{-}1.1\ g_M$, whereas that for $D = 1$ slope instability could be obtained with zero *Ru* or *SLC*. Otherwise, for slopes composed of non-welded tuffs and $Ru = 0$ and $SLC = 0\ g_M$ we obtain *SF* values between 1.1 and 2.4 and between 0.6 and 1.2 for, respectively, $D = 0$ and $D = 1$. For $D = 0$, instability could occur when $Ru > 0.2\text{-}0.7$ or $SLC > 0.07\text{-}0.3\ g_M$, whereas for $D = 1$, landslides could initiate when $Ru > 0.0\text{-}0.3$ or $SLC > 0.0\text{-}0.05\ g_M$. Thus, a slope lithology of non-welded tuff implies the more favorable condition for landslide initiation.

5 Discussion and conclusions

The results of the landslide models presented in this study vary widely according to pore fluid pressure and seismic ground acceleration as triggering factors.

For a slope composed of materials with geomechanical properties approximating those of partially-welded tuffs with porosity ranging from 14% to 42% (Aydan and Ulusay 2003) and fully saturated with water, the volume of water involved in a landslide would be significant. Such a large water volume would help explain the presence of flow morphologies similar to those found in the more distal areas of terrestrial landslides, related to the lubricating actions of

water (Weitz et al. 2003; De Blasio 2012). However, our findings indicate that in this case are not need large amounts of liquid water for slope failure, which would therefore imply the instability of the whole scarp complex of Valles Marineris. Therefore, the presence of flow-type movements in the distal areas of some of the landslides does not necessarily indicate the presence of liquid water at the moment of failure; indeed, post-failure speed could be as high as 400 km/h (De Blasio 2012), which would produce strong particle friction leading to the melting of ice contained in the failed material, and in turn making its behavior that of a viscous body.

For slopes formed by materials with geomechanical properties approximating those of basalt with low disturbance factors, the *Ru* necessary for failure rises to >0.8, corresponding to a situation of pore water over-pressure. However, if the amount of liquid water present in the Martian subsurface is as abundant as suggested by *Ru* values obtained for basalt (or gabbro) rock masses, the evidences for surface or subsurface liquid water (for example as valley or run-off morphologies, or collapsed terrains) during the times when the landslides occurred should be greater.

If most of the underground water is in solid state, the weight of this subsurface ice will increase the *SF* of the slopes due to the contributions of the stabilizing forces, contributing therefore to the slope stability. Given the climate conditions prevailing on Mars over the last billions of years (e.g., Shuster and Weiss 2005), any water existing in the upper crust during the formation of the studied landslides would have likely occurred in solid state. It has been suggested that this ice currently forms part of a cryosphere extending from the planet's surface to a depth of 9 km at the Martian equator (Clifford et al. 2010), thus fully comprising the sections of failed material in Valles Marineris. Although the thermal state of the martian crust most probably vary (and varied in the past) across the planet, paleo-heat flow estimates for the Valles Marineris region based on lithospheric strength (Ruiz et al. 2011) do not find specially high values for this region, and therefore average cryosphere depths could be representative here. Thus, it does not seem that the presence of subsurface water, whether liquid or solid, was necessary to trigger the landslides examined here.

Landslides could be seismically induced, regardless of the saturation conditions (Brunetti et al. 2014). Indeed, a possible triggering mechanism is the ground shaking produced by volcanic processes, tectonic activity or meteoritic impacts. The tectonic history of Mars suggests that ground acceleration could be a consequence of the activity of some of the faults observed in the Valles Marineris canyon system, although the tectonic activity that led to the formation of Valles Marineris has been reported to have ended around 3.5 Ga ago (Hartmann and Neukum 2001) while the more recent landslides are 100 Ma old (Quentin et al. 2004b). On the other hand, other studies indicate that tectonism contributed to the development of Valles Marineris in the Late Hesperian and likely the Amazonian Period (Schultz, 1991; Dohm et al., 2009; Anderson et al., 2001; Yin, 2012), though likely diminished when compared to earlier activity such as during the Late Noachian/Early Hesperian (Anderson et al.,, 2001; Dohm et al., 2001).

The ground acceleration generated by meteoritic impacts could be an important contributing factor given the density of craters around Valles Marineris. Further, the disturbance factor *D* could increase as the number of impacts in a given zone accumulates, considerably reducing the rock mass strength and favoring their failure. As previously suggested (e.g., Crosta et al. 2014), even the presence of impact craters prior to the formation of the valley itself could be a determining factor for the landslides observed in Valles Marineris, because these impact could have fractured, and hence weakened, the rock massif.

In conclusion, the presence of subsurface water does not seem necessary to trigger the failure of slope materials that are not too consolidated (perhaps even could produce an excessive instability of wall rock, inconsistent with the present-day morphology and configuration of the canyon system), while large amounts of water are necessary to promote failure of more consolidated, basalt-type, materials. The presence of water in solid state in fact would contribute to slope stability because it implies a higher rock weight. If there is limited to no geologically recent magmatic or tectonic activity in the region, then ground shaking caused by meteoritic impacts is a likely primary triggering mechanism for the landslides in Valles Marineris based on our results.

We thank the comments from James Dohm and an anonymous reviewer. Also, we would like to thank Federico Mansilla for his technical assistance during the realization of this work. Figure 1 and 3 were generated using the Generic Mapping Tools (Wessel et al., 2013). J.R. work was supported by a contract Ramón y Cajal at the Universidad Complutense de Madrid (UCM). This work has received funding from the European Union's Horizon 2020 Programme (H2020-Compet-08-2014) under grant agreement UPWARDS-633127, and from the Spanish Ministry of Economy and Competitiveness Projects CGL2011-23857 (MTDRES) and CGL2014-59363-P (AMARTE).

L.W. Abramson, T.S. Lee, S. Sharma, G.M. Boyce, Slope stability and stabilization methods, 2nd edn. (Wiley, New York, 2001), p.736

R.C. Anderson, J.M. Dohm, M.P. Golombek, A.F. Haldemann, B.J. Franklin, K.L. Tanaka, J. Lias, B. Peer, J. Geophys. Res. 106, 20563-20585 (2001)

A. Aydan, R. Ulusay, Eng. Geol. 69, 245-272 (2003)

F. Bigot-Cormier, D.R. Montgomery, Earth Planet. Sci. Lett. 260, 179–186 (2007)

W.B. Boynton, et al., Science 297, 81-85 (2002)

M.T. Brunetti, F. Guzzetti, M. Cardinelli, F. Fiorucci, M. Santangelo, P. Mancinelli, G. Komatsu, L. Borselli, Earth Planet. Sci. Lett. 405, 156-168 (2014)

M.G. Chapman, in Volcano-Ice Interactions on Earth and Mars, ed. by J.L. Smellie, M.G. Chapman (Geol. Soc. Spec. Publ. 202, 2002), pp. 273-203

S.M. Clifford, J. Lasue, E. Heggy, J. Boisson, P. McGovern, M.D. Max, J. Geophys. Res. 115, E07001 (2010)

G.B. Crosta, S. Utili, F.V. De Blaso, R. Castellanza, Earth Planet. Sci. Lett. 388, 329–342 (2014)

F.V. De Blasio, Planet. Space Sci. 59, 1384–1392 (2012)

J.M. Dohm, J.C. Ferris, V.R. Baker, R.C. Anderson, T.M. Hare, R.G. Strom, N.G. Barlow, K.L. Tanaka, J.E. Klemaszewski, D.H. Scott, J. Geophys. Res. 106, 32943-32958 (2001)

J.M. Dohm, et al., J. Volcanol. Geoth. Res. 185, 12-27 (2009)

G. Dromart, C. Quantin, O. Broucke, Geology 35, 363-366 (2007)

E. Eberhardt, Rock Mech. Rock Eng. 45, 981-988 (2012)

P. Frattini, G.B. Crosta, F. De Blasio, R. Castellanza, S. Utili, A. Lucas, Proc. Lunar Planet. Sci. Conf. 45th. Abstract 2024 (2014)

K.P. Harrison, R.E. Grimm, Icarus 163, 347-362 (2003)

W.K. Hartmann, G. Neukum, Space Sci. Rev. 96, 165-194 (2001)

E. Hoek, C. Carranza-Torres, B. Corkum, Proc. NARMS-TAC Conference 1, 267-273 (2002)

B.M. Hynek, R.J. Phillips, R.E. Arvidson, J. Geophys. Res. 108(E9), 5111 (2003)

G. Komatsu, G.G. Ori, P. Ciarcelluti, Y.D. Litasov, Planet. Space Sci. 52, 167-187 (2004)

A. Lucas, A. Mangeney, D. Mège, F. Bouchut, J. Geophys. Res. 116, E10001 (2011)

B.K. Lucchitta, A.S. McEwen, G.D. Clow, P.E. Geissler, R.B. Singer, R.A. Schultz, S.W. Squyres, in Mars, ed. by H.H. Kieffer, B.M. Jakosky, C.W. Snyder, M.S. Matthews (University of Arizona Press, Tucson, 1992) pp. 453-492

B.K. Lucchitta, U.S. Geol. Surv. Invest. Ser., I-2568 (1999)

N. Mangold, D. Baratoux, V. Frey, in Second International Conference on Mars Polar Science and Exploration, Vol. 1, p. 121 (2000)

A.S. McEwen, M.C. Malin, M.H. Carr, W.K. Hartmann, Nature 397, 584–586 (1999)

D.T. Möhlmann, Icarus 168, 318-323 (2004)

D.P. Neuffer, R.A. Schultz, Q. J. Eng. Geol. Hydroge. 39, 227–240 (2006)

A. Özsan, H. Basarir, Eng. Geol. 68, 319-331 (2003)

J.-P. Peulvast, D. Mège, J. Chiciak, F. Costard, P.L. Masson, Geomorphology 37, 329-352 (2001)

C. Quantin, P. Allemand, C. Delacourt, Planet. Space Sci. 52, 1011-1022 (2004a).

C. Quantin, P. Allemand, N. Mangold, C. Delacourt, Icarus 172, 555-572 (2004b)

J. Ruiz, P.J. McGovern, A. Jiménez-Díaz, V. López, J.-P. Williams, B.C. Hahn, R. Tejero, Icarus 215, 508-517 (2011)

R.A. Schultz, J. Geophys. Res. 96, 22777-22792 (1991)

R.A. Schultz, Planet. Space Sci. 46, 827-834 (1998)

R.A. Schultz, Geophys. Res. Lett. 29, 1932 (2002)

D.L. Shuster, B.P. Weiss, Science 309, 594-597 (2005)

D.E. Smith, et al., J. Geophys. Res. 106, 23,689-23,722 (2001)

V. Soukhovitskaya, M. Manga, Icarus 180, 348-352 (2006)

C.-Y. Wang, M. Manga, A. Wong, Icarus 175, 551-555 (2005)

J. Watkins, B.E. Elhmann, A. Yin, Geology 43, 107-110 (2015)

C.M. Weitz, T.J. Parker, M.H. Bulmer, F.S. Anderson, J.A. Grant, J. Geophys. Res. 108, 8082 (2003)

P. Wessel, et al., EOS Trans. AGU 94, 409-410 (2013)

A. Yin, Lithosphere 4(4), *286-330* (2012)

Fig. 1. Mars Orbiter Laser Altimeter (MOLA) topographic shaded relief map of the Valles Marineris region, showing the location of the studied landslides (hereafter referred after the canyon where the landslide is located): Ius Chasma landslide, Candor Chasma landslide, and Melas Chasma landslide. The context boxes show the location of, respectively, Figure 2a, 2b and 2c.

Fig. 2. CTX (MRO) mosaics of the studied landslides: (a) Ius Chasma landslide, (b) Candor Chasma landslide, and (c) Melas Chasma landslide (see Figure 1 for context). Black arrows show movement directions for respective landslides. Illumination from left in all the cases.

Fig. 3. Topographic profile model of the initial slope for each analyzed landslides, based on the MOLA topography of the adjacent, non-slipped, canyon walls. We also indicate the obtained failure surface, and the area (gray) of slipped material.

Table 1. Geomechanical parameters used in slope stability modelling. Modified from Neuffer and Schultz (2006). *GSI*: Geologic Strength Index; *UCS*: Uniaxial Compressive Strength; *mi*: material constant for intact rock; γ: unit weight; *c*: cohesion; φ: friction angle.

Lithology	*GSI*	*UCS* (MPa)	*mi*	γ (kN m^{-3})	*c* (MPa)	φ	Reference
Nonwelded tuff	55	6	8	5.4			Aydan and Ulusay (2003)
Welded tuff	12	12	10	6.8			Ozsan and Basarir (2003)
Hyaloclastite breccia	60	24	18	6.1			Neuffer et al. (2006)
Hyaloclastite fracture					0.11	18	Neuffer et al. (2006)
Basalt	43	142	25	9.1			Ozsan and Basarir (2003)
Gabbro	63	96	27	11.3			Wines and Lilly (2001)

Table 2. Results for the slope stability modeling with D = 0. (ss) means the surface was numerically calculated. *SF*: Safety Factor; *Ru*: water pressure; *SLC*: seismic load coefficient, which is given in g_M units.

Landslide	Lithology	*SF*	*Ru* (for *SF* = 1)	*SLC* (for *SF* = 1)
Ius Chasma	Nonwelded tuff	1.37	0.366	0.114
Ius Chasma	Welded tuff	0.877	0.000	0.000
Ius Chasma	Hyaloclastite breccia	3.100	0.738	0.580
Ius Chasma	Hyaloclastite fracture	1.096	0.083	0.290
Ius Chasma	Basalt	4.309	0.798	0.849
Ius Chasma	Gabbro	4.623	0.817	0.917
Ius Chasma (ss)	Nonwelded tuff	1.119	0.239	0.067
Ius Chasma (ss)	Welded tuff	0.786	0.000	0.000
Ius Chasma (ss)	Hyaloclastite breccia	2.752	0.697	0.569
Ius Chasma (ss)	Hyaloclastite fracture	0.805	0.000	0.000
Ius Chasma (ss)	Basalt	3.833	0.773	0.585
Ius Chasma (ss)	Gabbro	4.111	0.794	0.931
Candor Chasma	Nonwelded tuff	2.387	0.715	0.288
Candor Chasma	Welded tuff	1.526	0.454	0.112
Candor Chasma	Hyaloclastite breccia	5.269	0.884	0.823
Candor Chasma	Hyaloclastite fracture	1.686	0.411	0.145
Candor Chasma	Basalt	7.244	0.917	1.159
Candor Chasma	Gabbro	7.787	0.935	1.251
Candor Chasma (ss)	Nonwelded tuff	1.878	0.619	0.210
Candor Chasma (ss)	Welded tuff	1.232	0.265	0.056
Candor Chasma (ss)	Hyaloclastite breccia	4.340	0.869	0.764
Candor Chasma (ss)	Hyaloclastite fracture	1.328	0.256	0.086
Candor Chasma (ss)	Basalt	6.028	0.890	1.127
Candor Chasma (ss)	Gabbro	6.478	0.921	1.216
Melas Chasma	Nonwelded tuff	1.497	0.452	0.141
Melas Chasma	Welded tuff	0.974	0.000	0.000
Melas Chasma	Hyaloclastite breccia	3.419	0.791	0.633
Melas Chasma	Hyaloclastite fracture	1.257	0.197	0.072
Melas Chasma	Basalt	4.772	0.852	0.945
Melas Chasma	Gabbro	5.116	0.871	1.024
Melas Chasma (ss)	Nonwelded tuff	1.400	0.415	0.105
Melas Chasma (ss)	Welded tuff	0.931	0.000	0.000
Melas Chasma (ss)	Hyaloclastite breccia	3.309	0.794	0.593
Melas Chasma (ss)	Hyaloclastite fracture	1.009	0.009	0.003
Melas Chasma (ss)	Basalt	4.665	0.851	0.916
Melas Chasma (ss)	Gabbro	4.994	0.869	0.992

Table 3. Results for the slope stability modeling with D = 1. (ss) means the surface was numerically calculated. *SF*: Safety Factor ; *Ru*: water pressure; *SLC*: seismic load coefficient, which is given in g_M units.

Landslide	Lithology	*SF*	*Ru* (for *SF* = 1)	*SLC* (for *SF* = 1)
Ius Chasma	Nonwelded tuff	0.689	0.000	0.000
Ius Chasma	Welded tuff	0.168	0.000	0.000
Ius Chasma	Hyaloclastite breccia	1.877	0.567	0.261
Ius Chasma	Hyaloclastite fracture	1.096	0.083	0.029
Ius Chasma	Basalt	2.193	0.630	0.348
Ius Chasma	Gabbro	3.052	0.734	0.569
Ius Chasma (ss)	Nonwelded tuff	0.589	0.000	0.000
Ius Chasma (ss)	Welded tuff	0.146	0.000	0.000
Ius Chasma (ss)	Hyaloclastite breccia	1.659	0.511	0.218
Ius Chasma (ss)	Hyaloclastite fracture	0.805	0.000	0.000
Ius Chasma (ss)	Basalt	1.943	0.566	0.324
Ius Chasma (ss)	Gabbro	2.709	0.692	0.555
Candor Chasma	Nonwelded tuff	1.219	0.278	0.047
Candor Chasma	Welded tuff	0.294	0.000	0.000
Candor Chasma	Hyaloclastite breccia	3.237	0.798	0.453
Candor Chasma	Hyaloclastite fracture	1.686	0.411	0.143
Candor Chasma	Basalt	3.755	0.823	0.549
Candor Chasma	Gabbro	5.188	0.884	0.809
Candor Chasma (ss)	Nonwelded tuff	0.926	0.000	0.000
Candor Chasma (ss)	Welded tuff	0.229	0.000	0.000
Candor Chasma (ss)	Hyaloclastite breccia	2.529	0.747	0.375
Candor Chasma (ss)	Hyaloclastite fracture	1.328	0.256	0.086
Candor Chasma (ss)	Basalt	3.049	0.789	0.478
Candor Chasma (ss)	Gabbro	4.271	0.865	0.749
Melas Chasma	Nonwelded tuff	0.748	0.000	0.000
Melas Chasma	Welded tuff	0.183	0.000	0.000
Melas Chasma	Hyaloclastite breccia	2.057	0.633	0.292
Melas Chasma	Hyaloclastite fracture	1.257	0.197	0.072
Melas Chasma	Basalt	2.411	0.689	0.384
Melas Chasma	Gabbro	3.365	0.786	0.620
Melas Chasma (ss)	Nonwelded tuff	0.682	0.000	0.000
Melas Chasma (ss)	Welded tuff	0.171	0.000	0.000
Melas Chasma (ss)	Hyaloclastite breccia	1.952	0.626	0.250
Melas Chasma (ss)	Hyaloclastite fracture	1.009	0.009	0.003
Melas Chasma (ss)	Basalt	2.311	0.687	0.347
Melas Chasma (ss)	Gabbro	3.255	0.790	0.58

Figure 1

Click here to download Figure Figure_1.tif

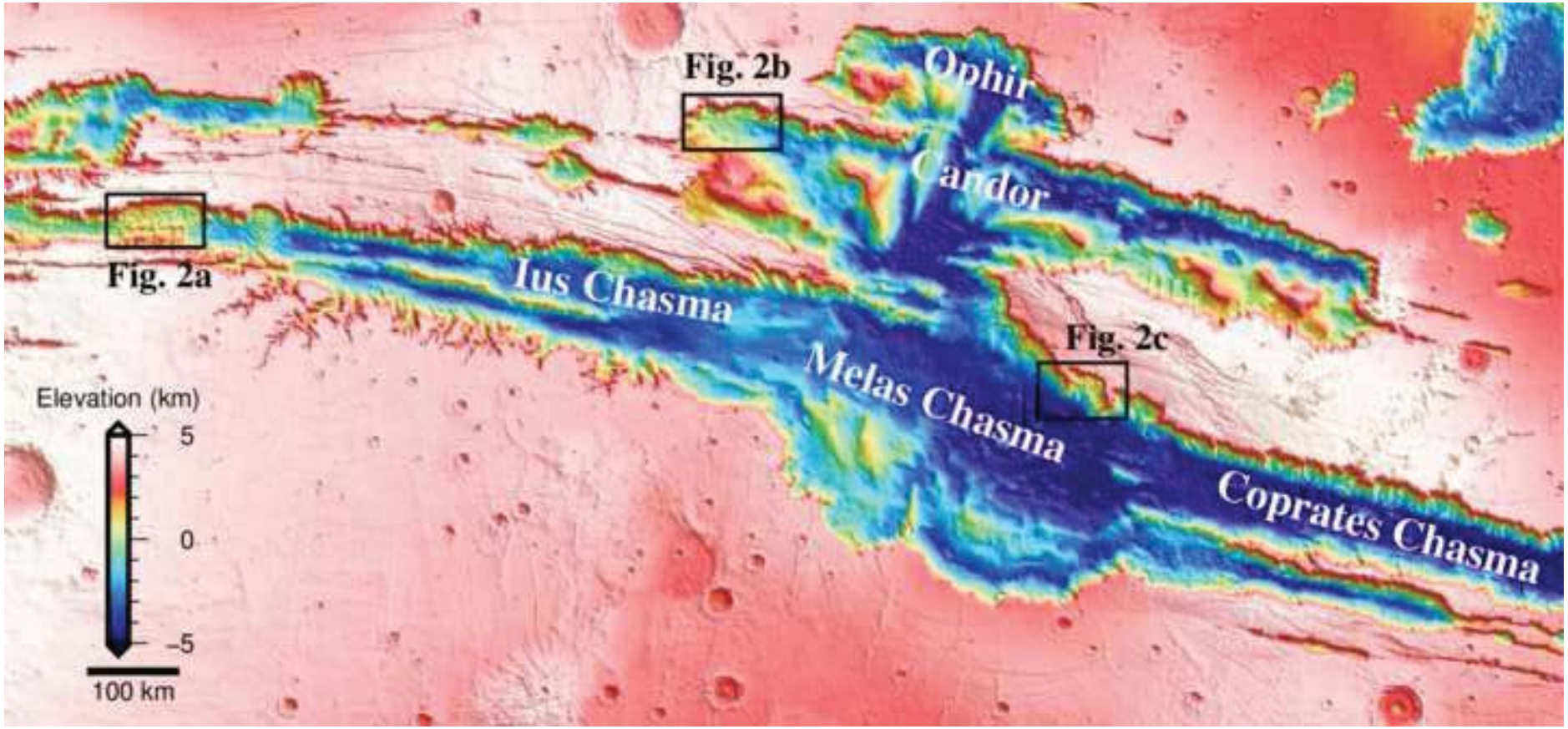

Figure 2

Click here to download Figure Figure_2.tif

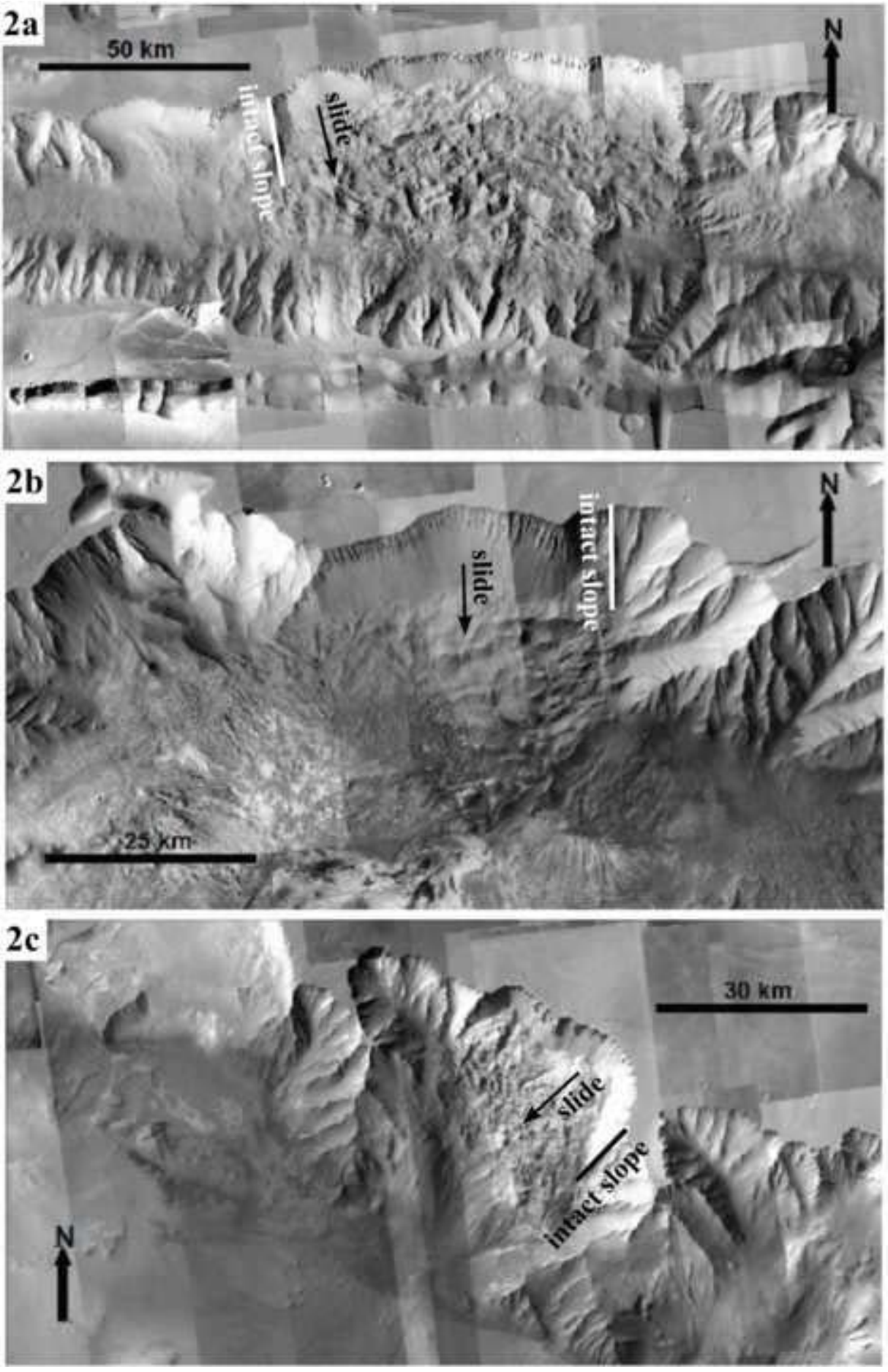

Figure 3

Click here to download Figure Figure_3.tif